Journal of Nuclear Medicine, published on July 16, 2021 as doi:10.2967/jnumed.121.261925

Fibroblast Activation Protein specific PET/CT imaging in fibrotic interstitial lung diseases and lung cancer: a translational exploratory study.

Running title: FAPI- PET/CT in fILD and LC

Manuel Röhrich[1], Dominik Leitz[2], Frederik M. Glatting[3], Annika K. Wefers[4], Oliver Weinheimer[2], Paul Flechsig[1], Nicolas Kahn[5], Marcus A. Mall[2], Frederik L. Giesel[1], Clemens Kratochwil[1], Peter E. Huber[3], Andreas von Deimling[4], Claus Peter Heußel[6], Hans Ulrich Kauczor[2], Michael Kreuter[2*] and Uwe Haberkorn[1*]

*equal senior authors

Affiliations:

1 Department of Nuclear Medicine, University Hospital Heidelberg, Germany

2 Translational Lung Research Center Heidelberg (TLRC), Member of the German Center for Lung Research DZL, Heidelberg, Germany

3 Clinical Cooperation Unit Molecular and Radiation Oncology, German Cancer Research Center (DKFZ), Heidelberg, Germany

4 Department of Neuropathology, Institute of Pathology, University of Heidelberg, Germany.

5 Centre for Interstitial and Rare Lung Diseases, Pneumology and Respiratory Critical Care Medicine, Thorax Clinic, University of Heidelberg, Germany

6 Diagnostic and Interventional Radiology with Nuclear Medicine, Thoraxklinik, University of Heidelberg, Heidelberg, Germany

Corresponding Author:

Manuel Röhrich

Im Neuenheimer Feld 400

69120 Heidelberg

Telephone: 0049 6221 56 7731

Fax: 0049 6221 56 5473

Email: manuel.roehrich@med.uni-heidelberg.de

ORCID-ID: 0000-0001-7609-243X

DECLARATIONS

Funding: This work was funded by the Federal Ministry of Education and Research, grant number 13N 13341.

Conflicts of interest: UH, CK and FLG have filed a patent application for quinoline based FAP targeting agents for imaging and therapy in nuclear medicine. UH, CK and FLG also have shares of a consultancy group for iTheranostics. No other potential conflicts of interest relevant to this article exist.

Ethics approval: All procedures performed in studies involving human participants were in accordance with the ethical standards of the institutional and/or national research committee and with the 1964 Helsinki declaration and its later amendments or comparable ethical standards. This retrospective study was approved by the local institutional review board (study number S-115/2020).

Animal studies: All animal studies were approved by the animal welfare authority responsible for the University of Heidelberg (Regierungspräsidium Karlsruhe, Karlsruhe, Germany).

ABSTRACT

Purpose:

Interstitial lung diseases (ILD) comprise over 200 parenchymal lung disorders. Among them, fibrosing ILDs, especially idiopathic pulmonary fibrosis (IPF) in particular are associated with a poor prognosis, while some others ILDs like sarcoidosis have a much better prognosis. A high proportion of ILD manifests as fibrotic ILD (fILD). Lung cancer (LC) is a frequent complication of fILD. Activated fibroblasts are crucial for fibrotic processes in fILD. The aim of this exploratory study was to evaluate the imaging properties of static and dynamic FAPI-PET/CT in various types of fILD and to confirm FAP expression of fILD lesions by FAP immunohistochemistry of human fILD biopsy samples and of lung sections of genetically engineered (Nedd4-2 -/-) mice with an idiopathic pulmonary fibrosis (IPF) -like lung disease.

Patients and Methods:

PET-Scans of 15 patients with fILD and suspected LC were acquired 10, 60 and 180 minutes after the administration of 150-250 MBq of a ^{68}Ga labelled FAPI tracer (FAPI-46). In three patients, dynamic scans over 40 mins were performed instead of imaging after 10 minutes. Standardized uptake values (SUVmax and SUVmean) of fibrotic lesions and LC were measured and CT-density-corrected. Target-to-background ratios (TBR) were calculated. PET imaging was correlated with CT-based fibrosis scores. Time-activity curves derived from dynamic imaging were analyzed. FAP immunohistochemistry of 4 human fILD biopsy samples and of fibrotic lungs of *Nedd4-2*$^{-/-}$ mice was carried out.

Results:

FILD lesions as well as LC showed markedly elevated FAPI-uptake (density corrected SUVmax / mean values 60 minutes post injection: 11,12 +/- 6,71 and 4,29 +/- 1,61 for fILD lesions and 16,69 +/- 9,35 and 6,44 +/- 3,29 for LC) and high TBR (TBR of density corrected SUVmax/SUVmean values 60 minutes post injection: 2,30 +/- 1,47 and 1,67 +/- 0,79 for fILD and 3,90 +/- 2,36 and 2,37 +/- 1,14 for LC). SUVmax and SUVmean values decreased over time with stable TBR of fILD and increasing TBR in LC on trend. Dynamic imaging showed differing time activity curves of fILD and LC. FAPI uptake

showed a positive correlation with the CT-based fibrosis index (FIBI). Immunohistochemistry of human biopsy samples and lungs of *Nedd4-2*$^{-/-}$ mice showed a patchy expression of FAP in fibrotic lesions, preferentially in the transition zone to healthy lung parenchyma.

Conclusion:

FAPI-PET/CT imaging is a promising new imaging modality for fILD and LC. Its potential clinical value for monitoring and therapy evaluation of fILD should be investigated in future studies.

Keywords: Fibroblast Activation Protein, Interstitial Lung Disease, Lung Cancer

BACKGROUND

Interstitial lung diseases (ILD) comprise over 200 parenchymal lung disorders. Among them, fibrosing ILDs, especially idiopathic pulmonary fibrosis (IPF) in particular are associated with a poor prognosis, while some others ILDs like sarcoidosis have a much better prognosis (*1,2*). A high proportion of ILD manifests as fibrotic ILD (fILD) with a potential of disease progression despite conventional therapy, which is associated with worsened lung function and quality of life as well as early death (*3*). Idiopathic pulmonary fibrosis (IPF) is a subtype of fILD with a typically chronic, irreversible and progressive clinical course (*4,5*), a variable disease course and a poor prognosis (*4,6,7*). But also in other fILDs including ILD associated with rheumatoid arthritis (RA-ILD) (*8*), systemic sclerosis associated ILD (SSc-ILD) (*9*) and unclassifiable Interstitial Lung Disease (uILD) (*10*) progressive fILD has been observed in a proportion of patients. Lung cancer (LC) is a frequent complication of fILD that crucially contributes to the poor prognosis of these patients (*11*).

The standard imaging technique for the assessment of fILD is high-resolution CT (HRCT) (*7*). CT is an essential component for the diagnosis of ILD and radiological patterns are predictors for outcomes and therapy effects *(12)*. Yet, CT is unable to assess disease activity in fILDs. Next to CT, ^{18}Fluor-Desoxy-Glucose (^{18}F-FDG) Positron Emission Tomography combined with Computed Tomography (PET/CT) is used for the imaging of fILDs, based on increased glucose metabolism in fibrotic pulmonary lesions (*13-16*), and may add additional value to CT for risk stratification and therapy evaluation of anti-fibrotic therapies (*13*). But both CT and FDG-PET have inherent limitations for the evaluation of fILDs as CT can only show morphological changes of the lung, which occur relatively late during fibrosis (*14*), and FDG-PET/CT depicts inflammatory reactions, but not an activated fibrotic process itself (*17,18*)**.**

There is growing evidence that activated fibroblasts play a crucial role for pathogenesis and progression of fibrotic processes in fILD (*15,19-21*). Activated fibroblasts contribute to various physiological and pathological processes including fibrosis, inflammation and cancer (*22,23*). They are characterized by expression of fibroblast activation protein (FAP). It has been shown that FAP can be specifically

targeted by radioactive tracer molecules (*24,25*). First pilot studies showed elevated uptake of FAPI tracers in various tumor entities (*25,26*). In these studies, elevated tracer uptake was not only observed in tumors, but also in reactive processes, fibrotic and inflammatory lesions (*27*).

Based on these findings, we hypothesized that FAPI-PET/CT may be a useful imaging/diagnostic tool for fILD. The aim of our analysis was to evaluate the imaging properties of static and dynamic FAPI-PET/CT in various types of fILD and to confirm FAP expression of fILD lesions by FAP immunohistochemistry of human fILD biopsy samples and of lung sections of genetically engineered (Nedd4-2 -/-) mice with an idiopathic pulmonary fibrosis (IPF).

PATIENTS AND METHODS

Study design and patient Characterization

This was an exploratory, hypothesis-generating, retrospective, translational study. The institutional review board approved this study (study number S-115/2020) and all subjects signed a written informed consent.

Between July 2018 and August 2019, 15 patients (aged 56 to 80 years, average 71.2 years) suffering from different fILD subtypes were examined by FAPI-PET/CT. These patients were selected out of a total of 1135 patients with suspected lung cancer, who were examined in our instiution between July 2018 and August 2019. Of these, 1104 (97.3%) were examined by FDG-PET/CT and 31 (2.7%) were examined by FAPI-PET/CT including the 15 patients suffering from fILD, which were retrospectively analyzed in this study. In all of these cases, the clinical indication for FAPI-PET/CT imaging was suspected LC. The individual decision for FAPI-PET/CT and not FDG-PET/CT for these patients was made by a local interdisciplinary tumor board due to our previous experiences with FAPI-PET/CT in LC (*28*) and potential diagnostic benefit for fILD. ILD diagnoses were made by an interdisciplinary team based on the clinical presentation and the radiological pattern on CT - and in 8/15 cases on additional lung biopsy - before PET imaging according to international guidelines (8). Biopsy samples of sufficient size for immunohistochemistry were available in 4 cases. Detailed clinical and pathological patient characteristics and imaging protocols of each patient are given in supplemental table 1.

Static and dynamic FAP-specific PET/CT imaging

Diagnostic imaging was performed under the conditions of the updated declaration of Helsinki, § 37 (unproven interventions in clinical practice) and in accordance to the German Pharmaceuticals Law §13 (2b) for medical reasons. The radiotracer FAPI-46 labeled with ^{68}Ga as previously described (*29*) was applied intravenously (80 nmol/GBq). Static PET/CT scans of 12 patients were performed 10, 60 and 180 minutes post tracer administration with a Biograph mCT Flow™ PET/CT-Scanner (Siemens Medical Solutions) using the following parameters: slice thickness of 5 mm, increment of

3-4 mm, soft-tissue reconstruction kernel, care dose. Immediately after CT scanning, a whole-body PET was acquired in 3D (matrix 200x200) in FlowMotion™ with 0.7 cm/min. The emission data were corrected for random, scatter and decay. Reconstruction was conducted with an ordered subset expectation maximization (OSEM) algorithm with 2 iterations/21 subsets and Gauss-filtered to a transaxial resolution of 5 mm at full-width half-maximum. Attenuation correction was performed using the low-dose non-enhanced CT data. For dynamic PET/CT Scans of 3 patients a list-mode acquisition of 40 minutes was performed as previously described (*30,31*) followed by static imaging after 60 and 180 minutes.

Computed Tomography (CT)

Non-enhanced full end-inspiratory thin-section low-dose CT was routinely performed in the supine position as previously described (*32*).Patients were scanned with a 128-slice Definition AS scanner (Siemens Healthcare AG, Forchheim, Germany) with a dose-modulated protocol at 120 kV, 40 mAs (effective), a collimation of 0.6 mm and a pitch of 0.8.

Image analysis and quantification

Volumes of Interest (VOIs) in PET data

The quantitative assessment of standardized uptake values (SUV) was done by consensus reading by MR (experienced nuclear physician with PET expertise of more than 3000 examinations), FMG (medical student) and UH (board certified nuclear physician) using a volume of interest (VOI) technique. For VOI of fibrotic areas, a 20 mm sphere was drawn within a total of 55 CT-morphologically typical fibrotic lesions. Tumor VOIs were defined by an automatic isocontour with a cut-off at 50% of SUVmax. SUV values of fibrotic areas and tumors were corrected for healthy appearing lung parenchyma as background (SUV/BG).

Density Correction of SUV values

To correct the signal intensity in FAPI-PET according to CT-density, SUV values of each voxel were corrected for the tissue fraction within the CT scans which were acquired during PET/CT scan according to an already published and validated method (*33,34*).

Dynamic PET imaging analysis

Time-activity curves (TAC) of FAPI-46 uptake were obtained by applying the VOIs of 14 fibrotic lesions and 3 tumors to the entire dynamic dataset. Derived from TAC, time to peak values (TTP: time in minutes from the beginning of the dynamic acquisition up to the SUVmax of the lesion) were calculated. Dynamic data analysis was done using PMOD software (PMOD Technologies Ltd, Zürich).

CT-based automatic lobe segmentation and FIB / GGO Indices

Lungs and individual lobes were fully automatically segmented on inspiratory non-enhanced thin-section CT images by the in-house program YACTA (Version 2.7.1.3) according to previous publications (*35,36*). We defined the fibrosis index (FIBI) as the percentage of lung voxels >-775 HU and the ground glass opacity index (GGOI) as the percentage of voxels in the HU interval [-885, -775]. FIBI and GGOI were calculated for each lobe separately.

Co-Registration studies of FAPI PET/CT Images and CT Images

To achieve anatomically identical segments of FAPI-PET/CT images and diagnostic CT images, both were co-registrated using 3DSlicer 4.6.2 (www.slicer.org). Firstly, the low dose CT images of the PET/CT were intramodally co-registrated with the CT images based on 11 manually selected anatomical landmarks using affine transformation. Secondly, the transformation was applied to the PET images to achieve intermodal co-registration. Co-registrated PET images and CT images were loaded into the PMOD software and SUVmean values were extracted from the same CT-based pulmonary lobe segmentations, which were used for GGO- and FIB-indexing. A representative example of the performed intermodal co-registration of high resolution computed tomography (HRCT) and FAPI-PET images is shown in supplemental figure 1.

Animal Studies

Animal studies were approved by the animal welfare authority responsible for the University of Heidelberg (Regierungspräsidium Karlsruhe, Karlsruhe, Germany). For animal studies, we used *Nedd4-2*$^{-/-}$ mice, an established animal model of an IPF–like lung disease (*37*). To induce the conditional deletion of *Nedd4-2*, 4- to 6-week-old mice were exposed to 1 mg/ml doxycycline hydrochloride (Sigma, Darmstadt, Germany) dissolved in a 5% sucrose solution supplied as drinking water in light-protected bottles. Doxycycline solutions were prepared freshly and changed at least every 3 days. For immunohistochemical studies, 4- to 6-week-old mice were treated for 3–4 months with doxycycline until clinically symptomatic and then sacrificed for tissue collection. Mice were housed in a specific pathogen-free animal facility and had free access to food and water.

Immunohistochemistry of human and mouse tissue

Sufficient biopsy tissue of fILD was available for 4 patients. The time interval between biopsy and FAPI-PET/CT was: 15,5 +/- 10,96 months. All samples were provided by the Tissue Bank of the National Center for Tumor Diseases (NCT) Heidelberg, Germany, in accordance with the regulations of the tissue bank and the approval of the ethics committee of Heidelberg University.

In human tissue, the primary anti-FAP antibody ab207178 (EPR20021; Abcam, Cambridge, UK) diluted 1:100 and the primary anti-α-SMA antibody ab5694 (Abcam, Cambridge, UK), diluted 1:200 were used and staining was performed as previously decribed (*38*). For animal tissue, we used the rabbit anti-FAP antibody ab53066 (Abcam, Cambridge, UK) and staining was performed as previously described (*37*). For FAP and α-SMA immunohistochemistry, negative controls were obtained by omitting the primary antibody. All images were scanned and digitalized using NanoZoomer S60 Digital slide scanner (Hamamatsu Photonics, Hamamatsu, Japan).

Statistical Analysis

We performed descriptive analyses for patients and their characteristics. For determination of SUVs, median and range were used. The correlation of FAPI-uptake within or outside the tumor and fibrotic lesions was determined by using two-sided t-test after testing for normal distribution. A P-value of <0.05 was defined as statistically significant. Pearson correlation analysis was performed between FAPI-PET parameters and GGOI/FIB scores. Excel 2010 was used for statistical analyses.

RESULTS

Static PET imaging

In static imaging, both fILD and LC lesions showed considerably elevated tracer uptake after 10, 60 and 180 minutes. Density corrected SUVmax and SUVmean values of fILD and LC lesions decreased over time, whereat the decrease was more pronounced in fILD compared to LC (figure 1A, B). Due to decreasing background activity over time (supplemental figure 2), fILD showed relatively stable target to background ratios (TBR), while the TBR (SUVmax and SUVmean) of LC showed a tendency to increase over time (figure 1C, D). A lesion-wise overview of all SUV values and TBR values is given in supplemental table 2. FAPI-46 uptake and TBR values (60 minutes p.i.) of IPF compared to fILDs did not significantly differ (see supplemental figure 3). Figure 2 shows an exemplary case of patient with clinically progressive RA-ILD and NSCLC. In this patient, fILD lesions were found in the middle lobe of the right lung and in the basal parts of the right lung. Both of these lesions showed elevated tracer uptake, whereat the uptake in the middle lobe was markedly increased compared to the basal parts, which may indicate that fILD was activated in the middle lobe. The tumor lesion was intensively FAPI-positive (figure 2A, B).

Dynamic PET imaging

TACs of fILD and LC differed significantly. FILD lesions showed an early peak correlated with the aortic perfusion peak, which was followed by slowly decreasing signal intensity over time. In contrast, LC showed an increasing TAC with a delayed peak followed by a gradual washout phase (figure 3A). These differences are reflected by delayed TTP in LC compared to fILD lesions (figure 3B).

Correlation of PET-imaging and FIB / GGO indices of pulmonary lobes

To correlate FAPI-PET signal intensities with CT-morphology based parameters, we correlated SUVmean values of 75 pulmonary lobes with corresponding FIB-indices and GGOI-indices. Hereby, density corrected SUVmean values showed a moderately positive correlation (r=0.57) with the FIB-index (figure 4A). The correlations of SUVmean

values and GGO index were moderately negative (r=-0.44) (figure 4B). Additional quartile-wise analysis of SUVmean values and FIB/GGO indices also displayed these correlations (see supplemental figure 4). Analysis of SUVmax values and FIB/GGO indices showed similar tendencies relative to the correlation of SUVmean values and FIB/GGO, but no strong or moderate correlations (r=0,13 for SUVmax versus FIB index and -0,19 for SUVmax versus GGO index, data not shown).Of note, the correlation of FIB index and GGO index was strongly negative (r=-0,75) in our dataset (figure 4C).

Immunohistochemistry of human fILD biopsies

In human fILD sections, we observed FAP-positive areas in the transition zone between healthy lung tissue and fibrotic areas. FAP-positive cells and αSMA positive cells were widely inversely distributed within the fibrotic sections. Of note, blood vessels in the fibrotic areas were FAP-negative. Figure 5A-C shows exemplary images of a FAP-positive fibrotic spot in a biopsy punch.

FAP expression in fibrotic lungs of Nedd4-2$^{-/-}$ mice

Immunohistochemistry of whole lung sections of *Nedd4-2*$^{-/-}$ mice with IPF–like lung disease showed differential expression of FAP in fibrotic lesions and in healthy lung parenchyma. While healthy lung parenchyma showed low FAP expression, fibrotic areas showed inhomogeneous FAP-positivity (supplemental figure 5A). Next to perivascular FAP-positivity (supplemental figure 5B), we found FAP overexpressed predominantly in the transition zone to normal parenchyma (supplemental figure 5C) similarly to the expression in human fILD tissue.

DISCUSSION

Potential role of FAPI-PET/CT for the management of fILD

Our results show that FAPI-PET/CT can be used for the visualization of fibrotic areas and LC lesions in patients with fILD. A potential role of FAPI-PET/CT for the management of fILD, particularly as a potential prognosticator and a probable value for the response evaluation of respective therapies, should be evaluated. Hereby, it will be of special interest which beneficial information FAPI-PET/CT may add to the gold standard modality CT and to ^{18}F-FDG-PET/CT. With respect to CT, we observed a positive correlation of FAP signal intensities with the CT-based FIB Index, which indicates that FAPI-PET and CT are in principle comparable in the detection of fILD. A potential benefit of FAPI-PET/CT compared to CT could be the distinction between inactive and activated, progressive fibrosis, as suggested by figure 2. ^{18}F-FDG-PET/CT has frequently been applied in patients with fILD (*13,33,39*). ^{18}F-FDG PET/CT is of prognostic value for fILD patients (*13,15*). However, it has recently been demonstrated that ^{18}F-FDG uptake is not changed after therapy with the antifibrotic drugs nintedanib or pirfenidone and ^{18}F-FDG uptake cannot predict treatment response (*33*). As FAPI-PET does not display elevated glucose metabolism, but visualizes reactive fibroblasts, key players of fibrosis, it may be more suitable for the imaging of fibrotic activity and the evaluation of therapy response than ^{18}F-FDG-PET, which only depicts the inflammatory component (*17,18*)**.** In a recent pilot study, Bergmann et al. could demonstrate in 21 patients suffering from the fILD subtype SSc-ILD that tracer accumulation in FAPI-PET/CT is associated with disease progression independent of established predictors of progression and that FAPI-uptake decreases after anti-fibrotic treatment (*40*). These findings strongly support the hypothesis that FAPI-PET/CT imaging reflects fibrotic activity in fILD and therefore is an extremely promising imaging modality for this disease. For future systematic evaluation of FAPI-PET/CT for fILDs, preclinical experiments including treatment and evaluation of the therapy response must precede human studies. The *Nedd4-2*$^{-/-}$ mouse model could be useful for such experiments, as we observed FAP-positive fibrotic pulmonary lesions in Nedd 4-2$^{-/-}$ mice with a similar expression pattern as in human fILD. Next to imaging of the fibrotic process itself, FAPI-PET/CT may serve as an excellent “all in one” monitoring tool for the detection of LC in

fILD patients, as recent studies showed the value of FAPI-PET/CT for the assessment of LC (*26,41*), which is confirmed by our data.

Imaging at different time points

FAPI-PET/CT is a promising imaging modality both for malignancies and for non-tumorous conditions. However, to date, it is not clear, which is the optimal time point of image acquisition for FAPI-PET/CT. In our study, we observed the highest tracer uptake of LC and fibrotic lesions at the earliest time point (10 minutes) and a decreasing uptake after 60 and 180 minutes. However, the TBR of LC showed a tendency towards increasing values over time. Fibrotic lesions showed a relatively stable TBR over time. This indicates that the washout in the LC lesions is slower than in lung tissue, and that the washout kinetics in the fibrotic lesions and in lung tissue do not differ significantly. These findings are in line with our recently published study, where we evaluated FAPI-Uptake over time in pancreatic ductal adenocarcinomas and pancreatitis (*27*). There, we observed slightly decreasing uptake, but increasing TBR values of the tumors over time and decreasing uptake of pancreatitis over time. The results of these studies on tumors and chronic inflammatory / fibrotic processes indicate that imaging and analysis of TBR at different time points could be helpful for the discrimination of malignant and chronic inflammatory or fibrotic FAPI-positive lesions.

Dynamic imaging

Next to imaging at different time points, dynamic PET imaging can deliver important additional information to static PET imaging, as it allows evaluating tracer uptake over time and washout processes for the characterization of PET-positive lesions. In brain tumor imaging with amino acid tracers, dynamic imaging is of great value for the differentiation of low grade versus high grade tumors and progress versus pseudoprogression (*42,43*). In this project, we publish the first clinical experiences with dynamic FAPI-PET/CT, which must be considered preliminary as they are based on a

small number of patients. But two hypotheses can be generated from our dynamic data of LC and fILD. The first thesis is: The peak of the uptake in LC lesions was between about 10 and 30 minutes and the washout in the blood is relatively fast in the first minutes and then the TAC of the blood volume is slowly decreasing. Therefore, it seems to be likely that the optimal imaging time point with the highest SUV values and best TBR for tumor lesions could be significantly earlier than 60 minutes post injection (p.i.)., which has been used in most studies in analogy to the common acquisition time point in ^{18}F-FDG-PET/CT. Imaging time points later than 60 minutes p.i. may lead to decreased SUV values, but even improved TBR. With respect to clinical practice, they are less favorable if the detection rate of tumor lesions should not be better than in earlier time points. Analyses of the detection rates and TBR at different time points up to 180 minutes p.i. are ongoing to define the optimal imaging time point for FAPI-PET/CT. The second thesis is: Time activity curves based on dynamic imaging data show that the activity in fibrotic lesions decreases relatively fast, comparable to the blood volume. In contrast, LC lesions showed a peak at about 10-30 minutes p.i. and then slowly decreasing activity over time. Thus, significantly decreasing activity over time within the first 40 minutes may indicate that a lesion is rather fibrotic than malignant and stable or only slightly decreasing activity may indicate that a lesion is rather malignant. Both theses need to be evaluated by future prospective studies on dynamic FAPI-PET/CT imaging with higher numbers of individuals with malignant tumors and non-cancer lesions.

Limitations

Despite the promising results of this analysis, a number of limitations must be mentioned. Firstly, the total number of 15 patients is relatively small and the number of patients examined by dynamic FAPI-PET/CT is only three, so that our data must be considered preliminary and conclusions should be drawn with caution based on our dataset. Another major limitation is that there is a certain heterogeneity in the patient population as we included various types off fibrotic ILDs. However, many fibrotic ILDs have similar detrimental outcomes as IPF when it comes to a progressive phenotype. This underscores the need to visualize disease activity in fibrotic ILDs. Moreover, subgroup analysis (FAPI-Uptake and TBR of IPF versus other fILDs, see supplemental

figure 3) of our dataset showed no significant differences between different types of ILDs. Nevertheless, our results need confirmation by studies with larger cohorts off ILD patients. Next, patients have undergone FAPI-PET/CT, but no corresponding ^{18}F-FDG-PET/CT, as two PET/CT examinations using ionizing radiation were not possible in the clinical setting of this project. Nevertheless, a systematic intra-individual comparison of FAPI-PET/CT and ^{18}F-FDG-PET/CT in fILD would be an interesting and relevant topic for future studies, especially as previous studies showed significant differences between these two tracers for the evaluation of malignant as well as non-malignant diseases. (*18,41,44*). Another limitation is that biopsies of fILD tissue significantly preceeded FAPI-PET-imaging and so no correlation between FAPI-PET signal intensities and immunohistochemical expression of FAP could be examined. FAPI-guided biopsies of fILD tissue and radiologic-pathologic correlations would be a promising approach for future studies of FAPI-PET in fILD.

CONCLUSION

FAPI-PET/CT is a promising new imaging modality for fILD and LC displaying activated fibroblasts that are involved in fibrotic processes as well as in desmoplastic reactions in tumors. Imaging at different time points and dynamic imaging provides additional information on tracer kinetics and may be helpful for the discrimination of malignant and non-malignant FAPI-positive lesions. The clinical value of FAPI-PET/CT for fILD as a potential predictor of prognosis and therapy response should be evaluated in future studies.

KEY POINTS

Question: Is FAPI-PET/CT a potential new imaging method for patients with fibrotic interstitial diseases?

Pertinent Findings: We did a retrospective analysis of FAPI-PET imaging of 15 patients with fibrotic interstitial lung disease and suspected lung cancer. Fibrotic areas and tumor lesions both showed elevated FAPI-uptake, but differential tracer kinetics.

Implications for Patient Care: FAPI-PET/CT is a promising imaging method for patients suffering from fibrotic interstitial lung diseases, which should be further investigated.

REFERENCES

1. Travis WD, Costabel U, Hansell DM, et al. An official American Thoracic Society/European Respiratory Society statement: Update of the international multidisciplinary classification of the idiopathic interstitial pneumonias. *Am J Respir Crit Care Med.* 2013;188:733-748.

2. Behr J, Prasse A, Wirtz H, et al. Survival and course of lung function in the presence or absence of antifibrotic treatment in patients with idiopathic pulmonary fibrosis: long-term results of the INSIGHTS-IPF registry. *Eur Respir J.* 2020;56.

3. George PM, Spagnolo P, Kreuter M, et al. Progressive fibrosing interstitial lung disease: clinical uncertainties, consensus recommendations, and research priorities. *Lancet Respir Med.* 2020;8:925-934.

4. Raghu G, Collard HR, Egan JJ, et al. An official ATS/ERS/JRS/ALAT statement: idiopathic pulmonary fibrosis: evidence-based guidelines for diagnosis and management. *Am J Respir Crit Care Med.* 2011;183:788-824.

5. Richeldi L, Collard HR, Jones MG. Idiopathic pulmonary fibrosis. *Lancet.* 2017;389:1941-1952.

6. Ley B, Collard HR, King TE, Jr. Clinical course and prediction of survival in idiopathic pulmonary fibrosis. *Am J Respir Crit Care Med.* 2011;183:431-440.

7. Raghu G, Remy-Jardin M, Myers JL, et al. Diagnosis of Idiopathic Pulmonary Fibrosis. An Official ATS/ERS/JRS/ALAT Clinical Practice Guideline. *Am J Respir Crit Care Med.* 2018;198:e44-e68.

8. Zamora-Legoff JA, Krause ML, Crowson CS, Ryu JH, Matteson EL. Progressive Decline of Lung Function in Rheumatoid Arthritis-Associated Interstitial Lung Disease. *Arthritis Rheumatol.* 2017;69:542-549.

9. Hoffmann-Vold AM, Allanore Y, Alves M, et al. Progressive interstitial lung disease in patients with systemic sclerosis-associated interstitial lung disease in the EUSTAR database. *Ann Rheum Dis.* 2020.

10. Guler SA, Ellison K, Algamdi M, Collard HR, Ryerson CJ. Heterogeneity in Unclassifiable Interstitial Lung Disease. A Systematic Review and Meta-Analysis. *Ann Am Thorac Soc.* 2018;15:854-863.

11. Kreuter M, Ehlers-Tenenbaum S, Palmowski K, et al. Impact of Comorbidities on Mortality in Patients with Idiopathic Pulmonary Fibrosis. *PLoS One.* 2016;11:e0151425.

12. Hansell DM, Goldin JG, King TE, Jr., Lynch DA, Richeldi L, Wells AU. CT staging and monitoring of fibrotic interstitial lung diseases in clinical practice and treatment trials: a position paper from the Fleischner Society. *Lancet Respir Med.* 2015;3:483-496.

13. Win T, Screaton NJ, Porter JC, et al. Pulmonary (18)F-FDG uptake helps refine current risk stratification in idiopathic pulmonary fibrosis (IPF). *Eur J Nucl Med Mol Imaging.* 2018;45:806-815.

14. Win T, Thomas BA, Lambrou T, et al. Areas of normal pulmonary parenchyma on HRCT exhibit increased FDG PET signal in IPF patients. *Eur J Nucl Med Mol Imaging.* 2014;41:337-342.

15. Nobashi T, Kubo T, Nakamoto Y, et al. 18F-FDG Uptake in Less Affected Lung Field Provides Prognostic Stratification in Patients with Interstitial Lung Disease. *J Nucl Med.* 2016;57:1899-1904.

16. Groves AM, Win T, Screaton NJ, et al. Idiopathic pulmonary fibrosis and diffuse parenchymal lung disease: implications from initial experience with 18F-FDG PET/CT. *J Nucl Med.* 2009;50:538-545.

17. Luo Y, Pan Q, Yang H, Peng L, Zhang W, Li F. Fibroblast activation protein targeted PET/CT with (68)Ga-FAPI for imaging IgG4-related disease: comparison to (18)F-FDG PET/CT. *J Nucl Med.* 2020.

18. Hao B, Wu X, Pang Y, et al. [(18)F]FDG and ([68)Ga]Ga-DOTA-FAPI-04 PET/CT in the evaluation of tuberculous lesions. *Eur J Nucl Med Mol Imaging.* 2020.

19. Kottmann RM, Kulkarni AA, Smolnycki KA, et al. Lactic acid is elevated in idiopathic pulmonary fibrosis and induces myofibroblast differentiation via pH-dependent activation of transforming growth factor-beta. *Am J Respir Crit Care Med.* 2012;186:740-751.

20. Bondue B, Sherer F, Van Simaeys G, et al. PET/CT with 18F-FDG- and 18F-FBEM-labeled leukocytes for metabolic activity and leukocyte recruitment monitoring in a mouse model of pulmonary fibrosis. *J Nucl Med.* 2015;56:127-132.

21. Visscher DW, Myers JL. Histologic spectrum of idiopathic interstitial pneumonias. *Proc Am Thorac Soc.* 2006;3:322-329.

22. Hamson EJ, Keane FM, Tholen S, Schilling O, Gorrell MD. Understanding fibroblast activation protein (FAP): substrates, activities, expression and targeting for cancer therapy. *Proteomics Clin Appl.* 2014;8:454-463.

23. Egger C, Cannet C, Gerard C, et al. Effects of the fibroblast activation protein inhibitor, PT100, in a murine model of pulmonary fibrosis. *Eur J Pharmacol.* 2017;809:64-72.

24. Lindner T, Loktev A, Altmann A, et al. Development of Quinoline-Based Theranostic Ligands for the Targeting of Fibroblast Activation Protein. *J Nucl Med.* 2018;59:1415-1422.

25. Loktev A, Lindner T, Mier W, et al. A Tumor-Imaging Method Targeting Cancer-Associated Fibroblasts. *J Nucl Med.* 2018;59:1423-1429.

26. Giesel F, Kratochwil C, Lindner T, et al. FAPI-PET/CT: biodistribution and preliminary dosimetry estimate of two DOTA-containing FAP-targeting agents in patients with various cancers. *J Nucl Med.* 2018.

27. Rohrich M, Naumann P, Giesel FL, et al. Impact of (68)Ga-FAPI-PET/CT imaging on the therapeutic management of primary and recurrent pancreatic ductal adenocarcinomas. *J Nucl Med.* 2020.

28. Kratochwil C, Flechsig P, Lindner T, et al. (68)Ga-FAPI PET/CT: Tracer Uptake in 28 Different Kinds of Cancer. *J Nucl Med.* 2019;60:801-805.

29. Loktev A, Lindner T, Burger EM, et al. Development of Fibroblast Activation Protein-Targeted Radiotracers with Improved Tumor Retention. *J Nucl Med.* 2019;60:1421-1429.

30. Rohrich M, Huang K, Schrimpf D, et al. Integrated analysis of dynamic FET PET/CT parameters, histology, and methylation profiling of 44 gliomas. *Eur J Nucl Med Mol Imaging.* 2018;45:1573-1584.

31. Kratochwil C, Combs SE, Leotta K, et al. Intra-individual comparison of (1)(8)F-FET and (1)(8)F-DOPA in PET imaging of recurrent brain tumors. *Neuro Oncol.* 2014;16:434-440.

32. Jobst BJ, Weinheimer O, Trauth M, et al. Effect of smoking cessation on quantitative computed tomography in smokers at risk in a lung cancer screening population. *Eur Radiol.* 2018;28:807-815.

33. Bondue B, Castiaux A, Van Simaeys G, et al. Absence of early metabolic response assessed by 18F-FDG PET/CT after initiation of antifibrotic drugs in IPF patients. *Respir Res.* 2019;20:10.

34. Holman BF, Cuplov V, Millner L, et al. Improved correction for the tissue fraction effect in lung PET/CT imaging. *Phys Med Biol.* 2015;60:7387-7402.

35. Konietzke P, Weinheimer O, Wielputz MO, et al. Validation of automated lobe segmentation on paired inspiratory-expiratory chest CT in 8-14 year-old children with cystic fibrosis. *PLoS One.* 2018;13:e0194557.

36. Wielputz MO, Eichinger M, Weinheimer O, et al. Automatic airway analysis on multidetector computed tomography in cystic fibrosis: correlation with pulmonary function testing. *J Thorac Imaging.* 2013;28:104-113.

37. Duerr J, Leitz DHW, Szczygiel M, et al. Conditional deletion of Nedd4-2 in lung epithelial cells causes progressive pulmonary fibrosis in adult mice. *Nat Commun.* 2020;11:2012.

38. Rohrich M, Loktev A, Wefers AK, et al. IDH-wildtype glioblastomas and grade III/IV IDH-mutant gliomas show elevated tracer uptake in fibroblast activation protein-specific PET/CT. *Eur J Nucl Med Mol Imaging.* 2019;46:2569-2580.

39. Fraioli F, Lyasheva M, Porter JC, et al. Synergistic application of pulmonary (18)F-FDG PET/HRCT and computer-based CT analysis with conventional severity measures to refine current risk stratification in idiopathic pulmonary fibrosis (IPF). *Eur J Nucl Med Mol Imaging.* 2019;46:2023-2031.

40. Bergmann C, Jörg H W Distler*, Christoph Treutlein, Koray Tascilar, Anna-Theresa Müller, Armin Atzinger, Alexandru-Emil Matei, Johannes Knitza, Andrea-Hermina Györfi, Anja Lück, Clara Dees, Alina Soare, Andreas Ramming, Verena Schönau, Oliver Distler, Olaf Prante, Philipp Ritt, Theresa Ida Götz, Markus Köhner, Michael Cordes, Tobias Bäuerle, Torsten Kuwert, Georg Schett, Christian Schmidkonz. ^{68}Ga-FAPI-04 PET-CT for molecular assessment of fibroblast activation and risk evaluation in systemic sclerosis-associated interstitial lung disease: a single-centre, pilot study. *Lancet Rheumatol* 2021;03.

41. Chen H, Pang Y, Wu J, et al. Comparison of [(68)Ga]Ga-DOTA-FAPI-04 and [(18)F] FDG PET/CT for the diagnosis of primary and metastatic lesions in patients with various types of cancer. *Eur J Nucl Med Mol Imaging.* 2020;47:1820-1832.

42. Langen KJ, Stoffels G, Filss C, et al. Imaging of amino acid transport in brain tumours: Positron emission tomography with O-(2-[(18)F]fluoroethyl)-L-tyrosine (FET). *Methods.* 2017;130:124-134.

43. Galldiks N, Lohmann P, Albert NL, Tonn JC, Langen KJ. Current status of PET imaging in neuro-oncology. *Neurooncol Adv.* 2019;1:vdz010.

44. Luo Y, Pan Q, Yang H, Peng L, Zhang W, Li F. Fibroblast Activation Protein-Targeted PET/CT with (68)Ga-FAPI for Imaging IgG4-Related Disease: Comparison to (18)F-FDG PET/CT. *J Nucl Med.* 2021;62:266-271.

45. Flaherty KR, Wells AU, Cottin V, et al. Nintedanib in Progressive Fibrosing Interstitial Lung Diseases. *N Engl J Med.* 2019;381:1718-1727.

Figure 1

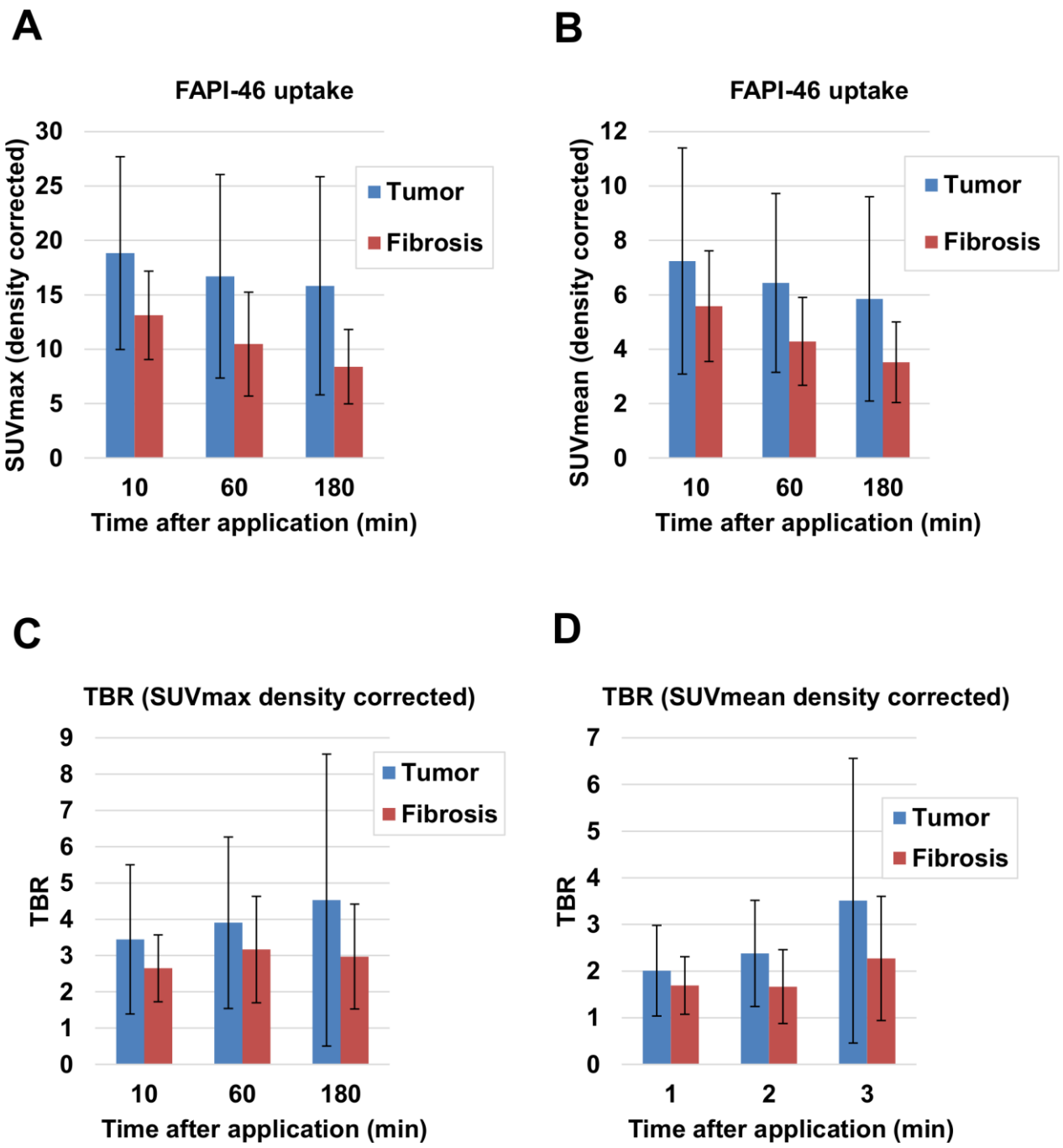

A, B Average density corrected SUVmax (A) and SUVmean (B) values +/- standard deviation for tumor and fibrosis in 15 patients 10, 60 and 180 minutes after application of FAPI-46. **C, D** Average density corrected tumor to background ratios of SUVmax (C) and SUVmean (D) +/- standard deviation for tumor and fibrosis in 15 patients 10, 60 and 180 minutes after application of FAPI-46.

Figure 2

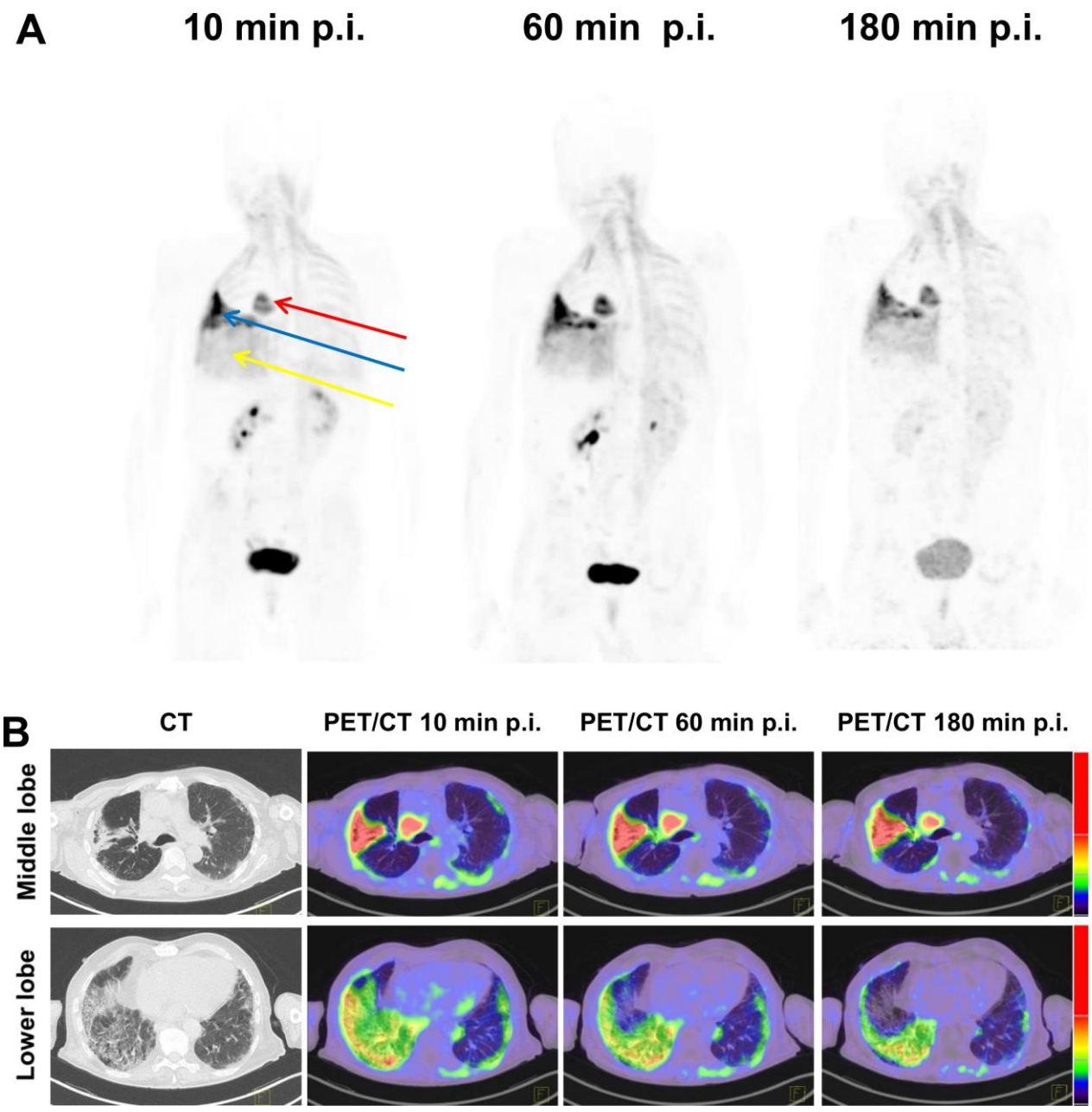

A Representative Mean Intensity Projection (MIP) Positron Emission Tomography (PET) images (10, 60 and 180 minutes after application of FAPI-46) of a 75 year old male patient suffering from RA-ILD and NSCLC (red arrow). Clinically, the patient had a significan decrease in forced vital capacity (from 70% to 38%) over the last 4 months before FAPI-PET/CT and complained about progressive weight loss and exertional dyspnea which denotes a progressive phenotype according to the criteria of the INBUILD study (*45*). We observed an intensively FAPI-positive pulmonary fibrosis in the

right middle lobe (blue arrow) and a moderately FAPI-positive pulmonary fibrosis in the right lower lobe (yellow arrow). **B** Representative axial Computed Tomography (CT)-images and fused PET/CT images (10, 60 and 180 minutes after application of FAPI-46) of the intensively FAPI-positive (upper row) and moderately FAPI-positive (lower row) pulmonary fibrosis lesions of the same patient. The intensively FAPI-positive lesion in the right middle lobe may be a correlate of increased fibrotic activity, leading to observed clinical progression of the fILD in this case.

Figure 3

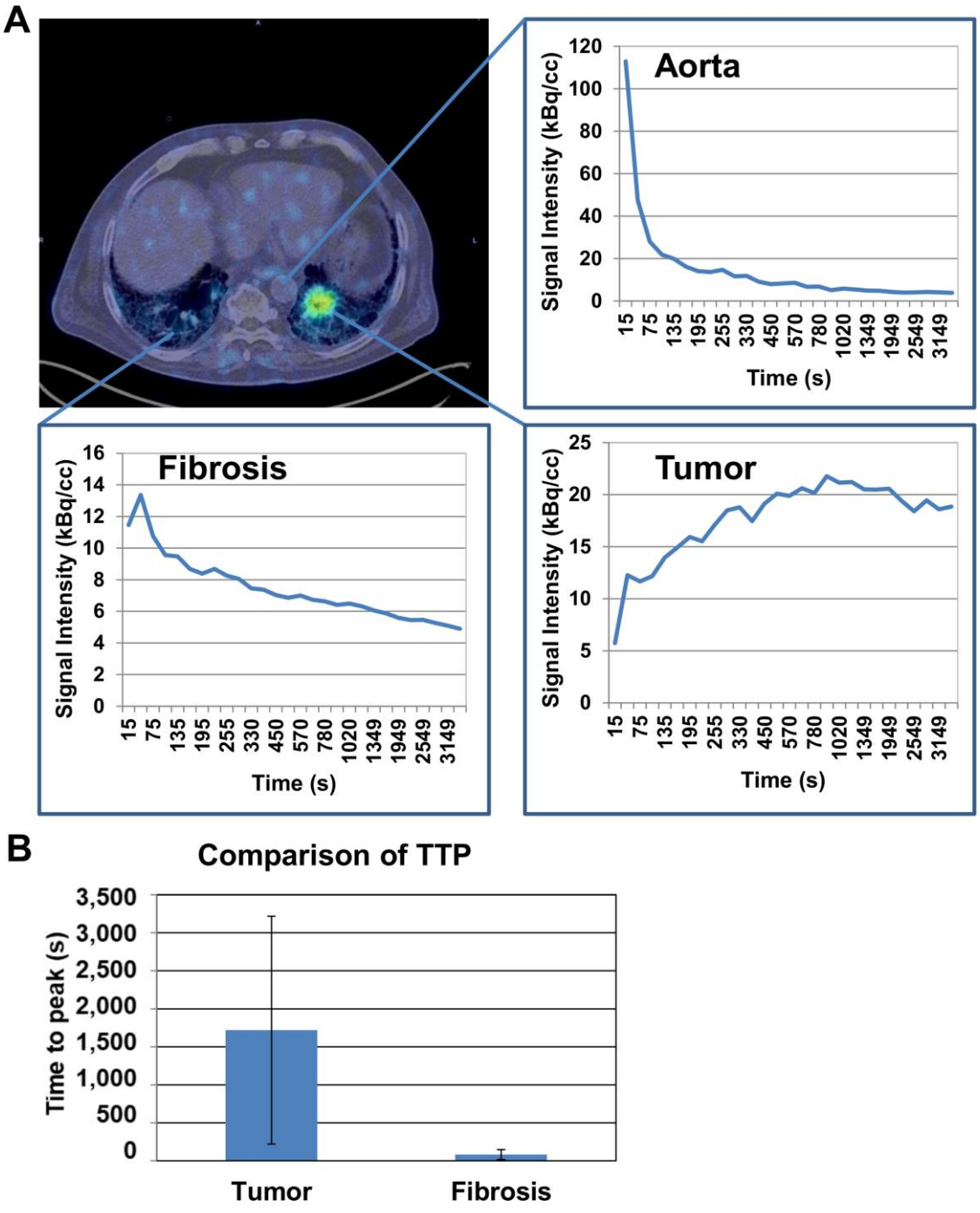

A An axial fused PET/CT image and corresponding TACs showing the uptake of FAPI-46 over time of the Aorta, a left-sided lung cancer lesion and a fibrotic area in the right lung. **B** Comparison of the average Time to Peak +/- standard deviation of three fibrotic areas and three lung cancer lesions as measured by dynamic PET-imaging.

Figure 4

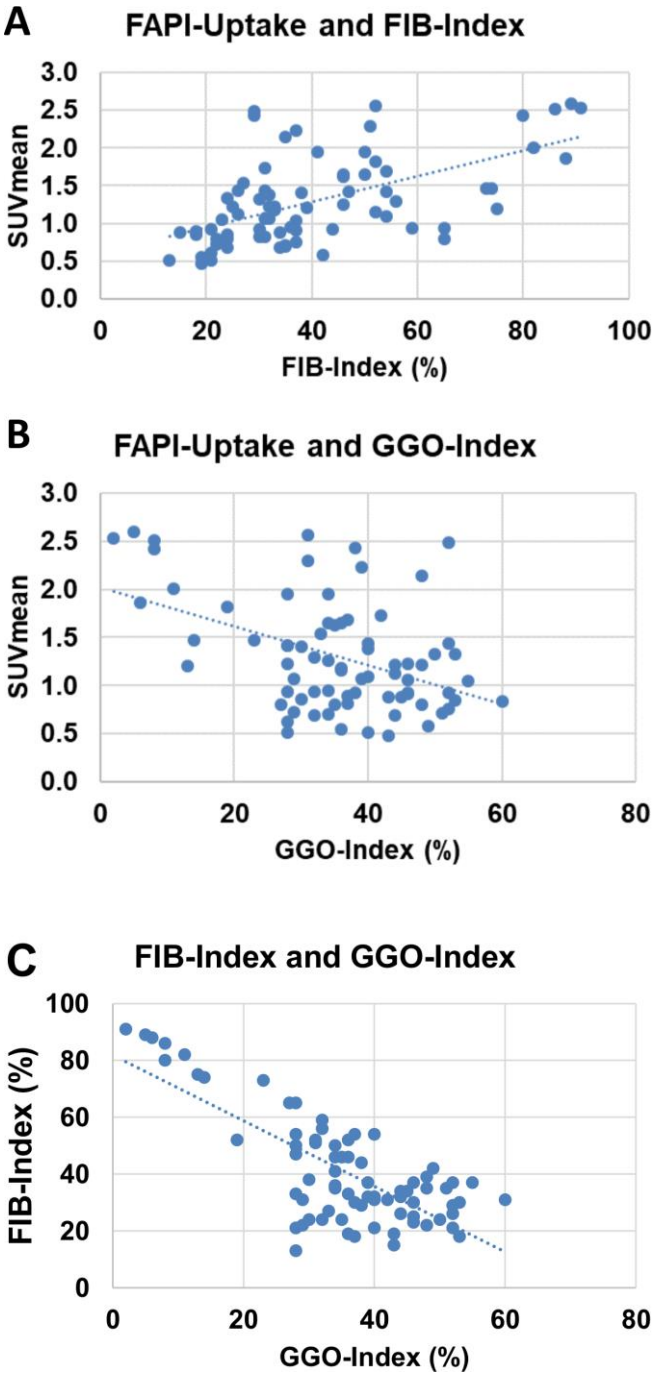

A,B Scatter plots of SUVmean values derived from FAPI-PET/CT and the corresponding FIB-Indices (**A**) and GGO Indices (**B**) in 75 lobe volumes of 15 patients with fILD and suspected LC. **C** Scatter plot of the FIB-Indices and GGO Indices of the same lobe volumes.

Figure 5

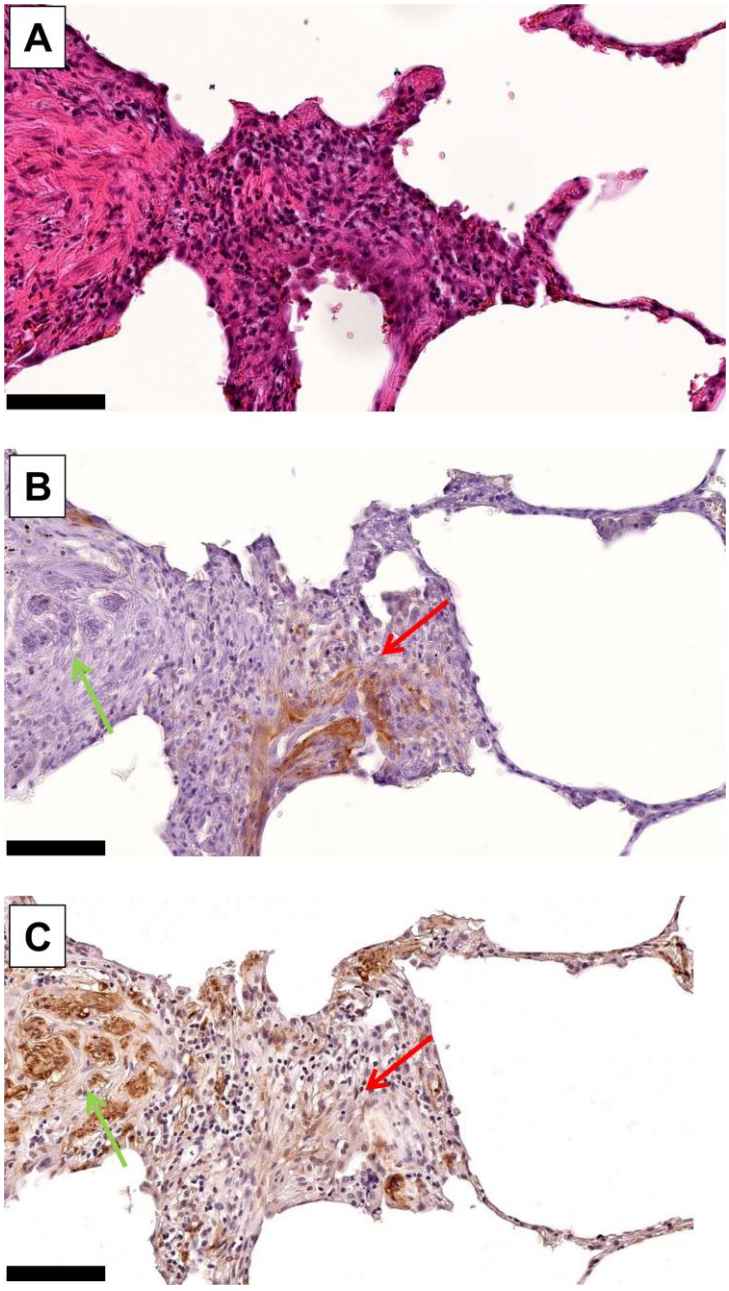

A-C-Hematoxylin and eosin (HE) staining (**A**), FAP-immunohistochemistry (**B**) and α SMA immunohistochemistry (**C**) of an exemplary FAP-positive spot in a fILD lesion of a 71 year old (time of biopsy) male patient suffering from IPF, who was diagnosed with SCLC after FAPI-PET/CT. High FAP-expression (red arrow) and high α SMA expression (green arrow) are widely inversely distributed in the fibrotic tissue. Magnification 20x, Scale bars: 50 μm.

GRAPHICAL ABSTRACT

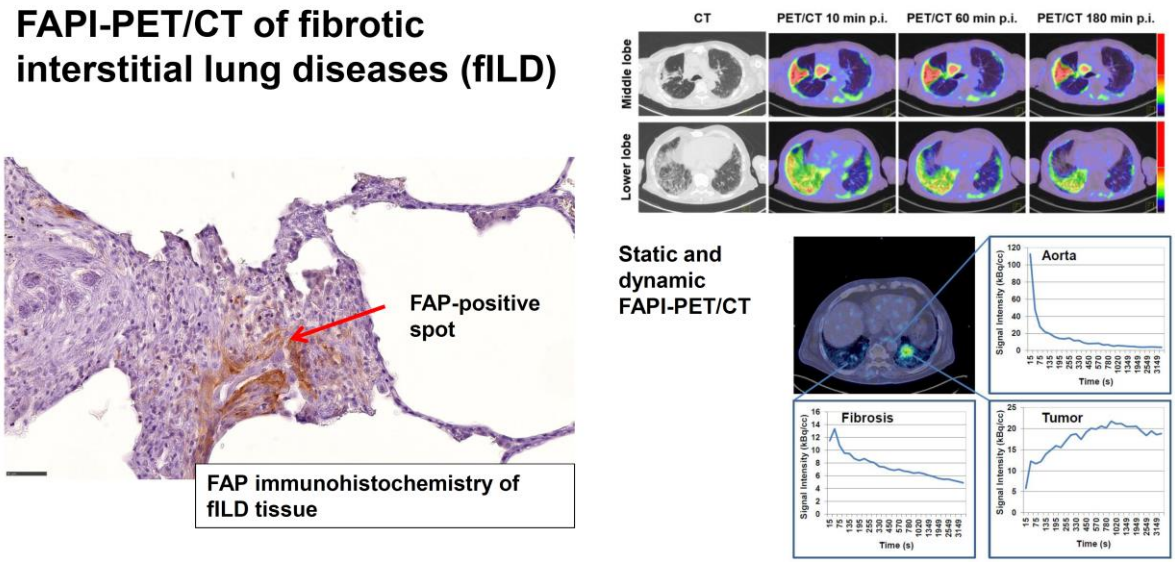

Supplemental Table 1: Clinical features and imaging protocols of 15 ILD patients with suspected lung cancer

No.	Age	Sex	FVC	DLCO	ILD Subtype	Biopsy technique	ILD pattern	LC Subtype	Tracer	Image acquisition p.i.
1	59	f	2,01 l (62,7%)	DLCO/SB 36,1 % DLCO/VA 61,3%	DIP	none		NSCLC (SCC)	FAPI-46	10,60,180 Min.
2	75	m	1,05 l (37,8%)	DLCO/SB 131,4% DLCO/VA 102,6%	RA-ILD	Surgical Biopsy	NSIP	NSCLC (SCC)	FAPI-46	10,60,180 Min.
3	69	m	2,13 l (51,7%)	DLCO/SB 21,6% DLCO/VA 39,9%	RA-ILD	none		NSCLC (SCC)	FAPI-46	10,60,180 Min.
4	69	f	1,79 l (69,8%)	DLCO/SB 51,5% DLCO/VA 75,6%	IPF	VATS and atypical resection of segments 2,9,10	UIP	LC not proven	FAPI-46	10,60,180 Min.
5	78	f	1,87 l (71,8%)	DLCO/SB 19,6 % DLCO/VA 30,6 %	SSc-ILD	Bronchoscopy	unspecific	LC not proven	FAPI-46	10,60,180 Min.
6	56	m	1,96 l (42%)	DLCO/SB 26,7% DLCO/VA 56,7%	uILD	Surgical Biopsy	UIP	NSCLC (AC)	FAPI-46	10,60,180 Min.
7	70	m	2,66 l (66,3%)	DLCO/SB 32% DLCO/VA 54,2%	IPAF	none		NSCLC (AC)	FAPI-46	10,60,180 Min.
8	76	m	2,33 l (66,6%)	DLCO/SB 36,6% DLCO/VA 66,6%	IPF	none		NSCLC (SCC)	FAPI-46	10,60,180 Min.
9	71	f	1,58 l (55,5%)	DLCO/SB 28,1%	IPF	Surgical Biopsy	UIP	NSCLC (AC)	FAPI-46	10,60,180 Min.
10	78	m	2,81 l (75,3%)	DLCO/VA 47,9%	IPF	Bronchoscopy	UIP	LC not proven	FAPI-46	10,60,180 Min.
11	74	m	3,07 l (80%)	DLCO/SB 28,2% DLCO/VA 45,4%	IPF	none		NSCLC (SCC)	FAPI-46	10,60,180 Min.
12	77	m	2,55 l (81,6%)	DLCO/SB 49,9% DLCO/VA 69,2%	IPF	1.Bronchoscopy	NSIP	SCLC	FAPI-46	10,60,180 Min.
						2. Surgical Biopsy	transition NSIP/UIP			
13	80	m	2,46 l (77,9%)	DLCO/SB 19,1% DLCO/VA 33,1%	CPFE	none		NSCLC (subtype not determined)	FAPI-46	dynamic 60 min. + 60,180 Min.
14	65	m	4,04 l (88,6%)	DLCO/SB 36,3% DLCO/VA 50,4%	IPAF	none		NSCLC (SCC)	FAPI-46	dynamic 60 min. + 60,180 Min.
15	71	m	3,54 l (96,5%)	DLCO/SB 49% DLCO/VA 62,5%	Sarcoidosis	TBB	epitheliod cell granuloma	LC not proven	FAPI-46	dynamic 60 min. + 60,180 Min.

Abbreviations: FVC = Forced Vital Capacity, DLCO = Diffusing Capacity of the Lung for Carbon Monoxide, VA = Alveolar Volume, SB = Single Breath, DIP = Desquamative Interstitial Pneumonia, RA-ILD = Rheumatoid Arthritis associated Interstitial Lung Disease, IPF = Idiopathic Pulmonary Fibrosis, IPAF = Interstitial Pneumonia with autoimmune Features, SSc-ILD = Systemic Sclerosis associated Interstitial Lung Disease, CPFE = Combined Pulmonary Fibrosis and Emphysema, uILD = unclassifiable Interstitial Lung Disease, LC = Lung Cancer, NSCLC = Non Small Cell Lung Cancer, SCC = Squamous Cell Carcinoma, AC = Adenocarcinoma, SCLC = Small Cell Lung Cancer, NSIP = Non Specific Interstitial Pneumonia , VATS = Video Assisted Thoracoscopic Surgery, UIP = Usual Interstitial Pneumonia

Supplemental table 2: density corrected SUV values and target to background ratios (TBR) off 55 fibrotic lesions in 15 patients with various fILD

Patient number	Localization of fibrotic lesion	10 minutes p.i.				60 minutes p.i.				180 minutes p..i.			
		SUV (density corrected)		TBR (density corrected values)		SUV (density corrected)		TBR (density corrected values)		SUV (density corrected)		TBR (density corrected values)	
		SUVmean	SUVmax	SUVmean	SUVmax	SUVmean	SUVmax	SUVmean	SUVmax	SUVmean	SUVmax	SUVmean	SUVmax
1	RUL	4.122470696	11.68574119	1.962224862	1.878182	3.88601749	10.2274065	1.81111161	2.62232856	0.74793642	2.01383798	3.87317147	3.72297669
	RML	4.844485338	12.35688173	2.305891363	1.986051	3.45704153	9.09536535	1.61118371	2.33207082	0.74793642	2.01383798	2.75963467	1.96869448
	RLL	4.564995799	11.88313546	2.172859169	1.909908	3.22993662	7.53392924	1.50533952	1.93171531	0.74793642	2.01383798	4.35731791	3.31364417
	LUL	4.937648518	12.63323372	2.350235428	2.030467	3.20470274	8.431755	1.49357906	2.16191973	0.74793642	2.01383798	4.35731791	3.39161227
	LLL	4.774612953	12.19896631	2.272633315	1.96067	3.93648525	9.13440125	1.83463254	2.3420797	0.74793642	2.01383798	4.06683005	2.86532761
2	RML	4.218142096	7.990471321	1.024096326	1.046341	3.36164571	5.49113451	1.53564214	1.57947595	1.07581006	2.4313868	3.15516662	2.2307032
	RLL	4.063550501	7.717504909	0.986564	1.010597	6.63304589	11.2329017	3.03005899	3.23104416	1.07581006	2.4313868	7.08619388	5.30651862
	LLL	4.151888555	6.104521568	1.008011043	0.799379	4.19641679	5.71898241	1.9169761	1.64501437	1.07581006	2.4313868	3.80171715	2.4468947
3	RUL	3.570303325	12.68122241	0.679657308	1.211729	3.32133585	10.8222836	0.85046987	1.37560588	2.58955338	4.913906	0.95352522	1.05556319
	RML	4.168285163	15.58733588	0.793491537	1.489417	4.55946696	10.7526869	1.16750893	1.36675954	2.58955338	4.913906	1.33493531	1.63237368
	RLL	5.680827458	17.56877688	1.081425174	1.67875	3.65543472	8.83877826	0.93602009	1.12348519	2.58955338	4.913906	1.10450005	1.48817106
	LUL	3.81653114	13.47379881	0.726530225	1.287462	3.55717035	9.46514838	0.91085826	1.20310225	2.58955338	4.913906	1.15217631	1.46509864
	LLL	3.939645048	16.11572014	0.749966684	1.539906	3.45890597	10.0219218	0.88569643	1.27387297	2.58955338	4.913906	1.13628422	1.44779432
4	RLL	4.046722708	17.69396194	1.745970137	5.000369	8.99848214	33.6942833	5.49016394	11.0113775	1.22178188	2.55056305	6.91754103	10.2353397
	LUL	3.139698653	9.475269445	1.354632003	2.677741	3.70940565	12.8344861	2.2631867	4.1943427	1.22178188	2.55056305	3.38303102	4.24241446
5	RLL	4.661628294	14.03888644	1.722838235	3.190291	2.01690117	6.46232909	1.23055399	2.11190558	1.22178188	2.55056305	1.57790626	2.18298997
	LLL	4.747162759	13.30608742	1.754449946	3.023765	4.00688272	10.1268618	1.69779912	1.48192986	1.40804307	3.79921345	1.85937706	1.96582597
6	RML	5.891261082	13.57279944	1.472390695	2.156954	4.58927846	12.0557879	1.94457224	1.76420221	1.40804307	3.79921345	2.78906559	2.72594534
	RLL	5.917918372	15.14353884	1.479053096	2.406572	3.38248143	8.97847767	1.00078445	2.13094315	1.98725405	3.66242613	1.30629885	1.79627981
	LUL	5.384772572	11.9215093	1.345805069	1.894535	4.22297681	12.9647727	1.24946422	3.07704654	1.98725405	3.66242613	1.43882192	2.03263242
	LLL	5.731317342	15.50601717	1.432416287	2.464176	3.44398109	10.8039773	1.01898053	2.56420545	1.98725405	3.66242613	1.25896918	1.72537403
7	RUL	7.544836319	13.72034047	2.891304038	3.537077	4.05897771	10.8412324	1.20094134	2.57304754	1.98725405	3.66242613	1.70386806	3.0016781
	LUL	7.049468278	13.45043214	2.701470945	3.467495	3.13971578	6.27657323	1.19816576	1.55562785	1.87110078	3.98712383	1.79081261	2.3206437
8	RUL	5.409333836	12.52043519	1.388010343	1.621334	2.97446758	6.87653979	1.1351044	1.70432757	1.87110078	3.98712383	1.38879345	2.39771305
	LLL	5.278673598	9.793922084	1.354483523	1.268264	3.85579131	8.16877546	1.47143163	2.02460389	1.87110078	3.98712383	1.42534065	2.3206437
9	RUL	4.935572787	10.6378189	1.376513778	1.275758	3.45185127	7.79956527	1.31728165	1.93309637	1.87110078	3.98712383	1.47407024	1.97811327
	RLL	5.335754364	11.08730421	1.488123003	1.329663	5.18778762	9.81753519	3.00397814	3.77946757	1.10196147	3.52202069	3.50531972	2.16684449
	LLL	6.936480673	14.87047219	1.934559904	1.783365	4.49608261	8.11647711	2.60344772	3.12460933	1.10196147	3.52202069	2.98874628	1.77630856
10	RML	4.520426488	10.25791396	2.051069705	2.638895	2.73744518	6.60620458	1.06386455	1.25176588	1.24265568	3.05452265	1.76430672	2.33434146

	LUL	4.081299344	9.278942922	1.851822934	2.38705	2.29091157	5.32964331	0.89032636	1.00987876	1.24265568	3.05452265	1.43104879	1.76432785
	LLL	5.631159854	15.87635647	2.555046833	4.084265	4.07566794	11.6055494	1.21817086	1.61116341	2.52724263	6.28504238	1.39104328	1.08422616
11	RUL	13.26554698	27.02917417	2.789810246	3.254479	4.51565482	12.2583615	1.34967794	1.70179135	2.52724263	6.28504238	1.71779841	1.30410419
	RML	6.893906306	12.4965015	1.449822647	1.504656	5.5114146	13.5277185	1.64729923	1.87801235	2.52724263	6.28504238	1.91385149	1.49365421
	RLL	9.470416744	16.72854354	1.991675556	2.01422	3.93672472	11.1340739	1.17664231	1.5457099	2.52724263	6.28504238	1.29768467	1.03494315
	LUL	9.365963618	20.60126126	1.969708546	2.480519	5.09458493	12.2220942	1.52271358	1.69675647	2.52724263	6.28504238	1.60576808	1.35338719
	LLL	8.216979233	15.5307958	1.728071438	1.870004	5.91264898	13.0487629	2.54446124	3.70166767	1.64521978	4.34116624	1.78385879	2.05313375
12	RUL	9.653535333	20.4482863	3.183644091	3.756101	5.05531487	11.3557272	2.17551436	3.221388	1.64521978	4.34116624	1.8266714	2.09663235
	RML	5.961169284	10.93366844	1.965936904	2.008381	6.6517301	16.0218988	2.8625189	4.54508562	1.64521978	4.34116624	2.29761012	2.45332084
	RLL	5.071442525	8.653882257	1.672513485	1.589613	3.3176141	7.51761926	2.41071133	2.1790841	0.68725643	1.57606631	3.61316584	4.71039972
	LUL	3.358718514	6.490411693	1.107673405	1.192209	2.84703054	6.33627909	2.06876646	1.8366566	0.68725643	1.57606631	2.3564125	2.82623983
	LLL	4.470876963	8.653882257	1.474452678	1.589613	3.22349739	7.01644464	2.34232235	2.03381183	0.68725643	1.57606631	3.17330217	3.48997798
13	RUL	not available due to dynamic imaging				10.7334511	27.5973769	2.92971336	4.53396979	2.30639047	6.00683043	3.99260191	2.8487371
	RML					5.56549317	14.8813245	1.51911063	2.44485104	2.30639047	6.00683043	1.58494197	1.11981607
	RLL					5.59199552	11.8893122	1.52634449	1.95329369	2.30639047	6.00683043	2.06889372	1.63052716
	LUL					5.45948378	11.6137321	1.49017519	1.90801867	2.30639047	6.00683043	1.59704076	1.12918691
	LLL					5.88352135	14.4089015	1.60591695	2.36723672	2.30639047	6.00683043	1.70592991	1.20415368
14	RUL					2.88450383	10.2565275	1.21523553	2.1646621	1.98768803	5.43846679	1.28169953	1.38120667
	RLL					2.96644997	10.3970279	1.24975927	2.194315	1.98768803	5.43846679	1.43248771	1.44274559
	LUL					2.14698865	8.25439711	0.9045219	1.74210819	1.98768803	5.43846679	1.28169953	1.38120667
	LLL					3.06478532	11.0995297	1.29118775	2.34257953	1.98768803	5.43846679	1.79689248	1.91454391
15	RUL					7.75435833	12.8538635	2.34724603	2.39671904	2.67409064	7.72851975	2.5473222	1.94894304
	RML					4.83507049	7.36699043	1.46357693	1.37364195	2.67409064	7.72851975	1.58624459	1.41089128
	RLL					4.81226355	7.42454504	1.45667327	1.38437353	2.67409064	7.72851975	1.53959034	1.27936752
	LUL					3.05612946	5.16073027	0.92509108	0.96226481	2.67409064	7.72851975	1.03572441	0.91269521
	LLL					3.92279304	6.08160408	1.18743034	1.13397005	2.67409064	7.72851975	1.32498078	1.10798807
Abbreviations: p.i. = post injection, RUL = right upper lobe, RML = right middle lobe, RLL = right lower lobe, LOL = left upper lobe, LLL = left lower lobe													